JOURNAL OF SPACECRAFT AND ROCKETS
Vol. 46, No. 3, May–June 2009

Flare-Type Membrane Aeroshell Flight Test at Free Drop from a Balloon

Kazuhiko Yamada,* Daisuke Akita,† Eiji Sato,‡ and Kojiro Suzuki§
University of Tokyo, Tokyo 113-8656, Japan
Tomohiro Narumi¶
Kyushu University, Fukuoka 812-8581, Japan
and
Takashi Abe**
Japan Aerospace Exploration Agency, Kanagawa 229-8510, Japan

DOI: 10.2514/1.40912

A space vehicle with a large-area, low-mass membrane aeroshell has potential as a reentry system in the near future, because the large-area, low-mass membrane aeroshell dramatically reduces aerodynamic heating and achieves a soft landing without a conventional parachute system. To demonstrate membrane aeroshell technology, a drop flight test of a capsule-type experimental flight vehicle with a 1.5-m-diam, flare-type, flexible, deployable membrane aeroshell was carried out using a large scientific balloon. In this flight test, the experimental flight vehicle was dropped from the balloon at an altitude of 39 km and underwent free flight. The flight data collected using onboard sensors were transmitted successfully during the flight by the telemetry system. The data showed that the vehicle was stable in free-flight condition and that its flight path and aerodynamic characteristics agreed well with results from previous trajectory analysis and wind-tunnel tests. This test flight clearly demonstrated that this flare-type flexible aeroshell successfully functions as a stable decelerating device in free flight.

Nomenclature

a_z = vertical acceleration of the vehicle, m/s^2
C_{AE} = aeroelasticity parameter
C_D = drag coefficient
d = distance from the center of view, m
E = Young's modules of the membrane, N/m^2
f = frequency of the aeroshell (3 Hz for aeroshell oscillation and 9 Hz for membrane fluttering)
h = thickness of the membrane, m
L_f = focal length of fish-eye lens, m
L_{ref} = referential length and diameter of the aeroshell, m
m = mass of the experimental vehicle, 106 kg
S_{ref} = referential area of the experimental vehicle, 1.64 m^2
St = Strouhal number
V_z = vertical velocity of the vehicle, m/s
V_{ter} = terminal velocity in the flight test, 31 m/s
V_∞ = freestream velocity, m/s
θ = elevation angle, rad
ρ_∞ = freestream density, kg/m^3

Received 10 September 2008; revision received 2 February 2009; accepted for publication 3 February 2009.

*Graduate Student, Department of Aeronautics and Astronautics, Graduate School of Engineering; currently Assistant Professor, Institute of Space and Astronautical Science, Japan Aerospace Exploration Agency, 3-1-1 Yoshinodai, Sagamihara 229-8510. Member AIAA.

†Graduate Student, Department of Advanced Energy, Graduate School of Frontier Science; currently Invited Researcher, Institute of Space and Astronautical Science, Japan Aerospace Exploration Agency, 3-1-1 Yoshinodai, Sagamihara 229-8510. Member AIAA.

‡Graduate Student, Department of Aeronautics and Astronautics, Graduate School of Engineering; currently Tokyo Instruments, Inc.

§Associate Professor, Department of Advanced Energy, Graduate School of Frontier Science, 5-1-5 Kashiwanoha, Kashiwa 277-8561. Member AIAA.

¶Graduate Student, Department of Aeronautics and Astronautics, Facility of Engineering; currently Postdoctoral Researcher, Department of Aerospace Engineering, Graduate School of Engineering, Tohoku University, 6-6-01 Aza Aoba, Sendai, Miyagi 980-8579.

**Professor, Institute of Space and Astronautical Science, 3-1-1 Yoshinodai, Sagamihara. Member AIAA.

I. Introduction

RECENTLY, construction of a lunar base and subsequent manned planetary exploration have attracted worldwide attention. The era for cargo and passenger shuttles between Earth and space is rapidly approaching, and thus the demand is strong for innovative space transportation systems to realize this vision. In particular, the development of low-cost, safe, reentry systems is crucial. A candidate for an innovative reentry system is a flexible aeroshell as a decelerator and recovery device from space [1]. A large, low-mass, flexible aeroshell, which enables the vehicle to decelerate at high altitude, where atmospheric density is very low, can dramatically reduce the aerodynamic heating of the space vehicle during reentry, because of a low ballistic coefficient. Furthermore, such a large aerodynamic surface can be used for the final deceleration before touchdown, because the terminal velocity of the space vehicle would also be reduced by this large aeroshell. Consequently, a soft landing could be achieved without a conventional parachute. Figure 1 outlines such a reentry and/or recovery system that uses a flexible aeroshell. This concept is expected to be cheaper and safer than traditional reentry and/or recovery systems, because the thermal protection system and the critical operation just before landing are significantly simplified.

Since 1960, various kinds of flexible aeroshells for spacecraft have been proposed for use in aeroassisted orbit transfer for planetary exploration: for example, as aerocapture or aerobraking [2]. Some countries are now considering applications of a flexible aeroshell to a reentry system, being attracted to the aerodynamic heating reduction effect due to a low ballistic coefficient. Since 1998, in collaboration with Russia, the European Space Agency has been developing the Inflatable Reentry and Deceleration Technology (IRDT) [3]. Three demonstration flights of IRDT reentry were, respectively, carried out in 2000, 2002, and 2005. Not all of the demonstration flights were successful, however, due to problems in the separation system and tracking system. NASA Langley Research Center has planned the Inflatable Reentry Vehicle Experiment (IRVE) using a sounding

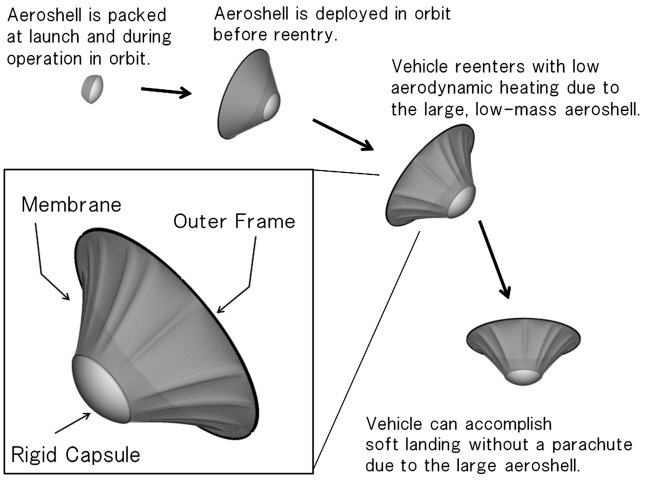

Fig. 1 Schematic of the reentry process using the flare-type membrane aeroshell.

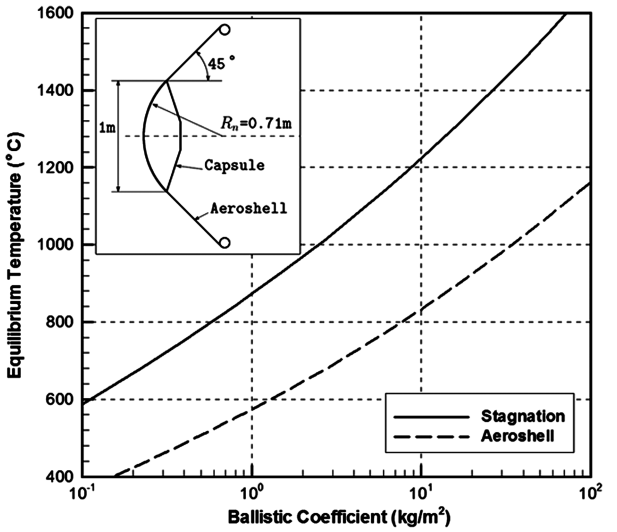

Fig. 2 Relation between ballistic coefficient and maximum equilibrium temperature at the stagnation point and the flare-type aeroshell estimated using trajectory simulation.

rocket [4]. Both systems adopt the clamped conical ballute-type aeroshell, which is deployed and sustained by gas pressure. (These systems are slightly complex and fragile, because a gas control system and a gas-tight aeroshell are necessary to maintain the configuration of the aeroshell.)

Our research group has developed another type of flexible aeroshell: namely, a flare-type membrane aeroshell derived from the tension-shell structure [5]. As shown in Fig. 1, the flare-type membrane aeroshell composed of a conical membrane and a ring-shaped outer frame is attached to a blunt rigid capsule, in which instruments for flight control (e.g., sensors, telemetry system, and batteries) and payload are installed. The advantages of this configuration are that only tensile forces act on the conical membrane, due to the aerodynamic force, and that this tensile force is compensated by the compression force acting on the outer frame. This configuration makes this aeroshell simpler and lighter than the ballute-type aeroshell, because, except for the outer frame, the aeroshell can be composed of a thin membrane.

However, it has never been demonstrated that the flare-type membrane aeroshell can maintain its configuration with the aerodynamic force and can function as a stable decelerator in complete free-flight condition. In this study, a flight test of a capsule-type experimental vehicle with a 1.5-m-diam flare-type membrane aeroshell was carried out using a large scientific balloon to investigate the behavior and aerodynamic characteristics of the capsule-type vehicle with the flare-type membrane aeroshell in free-flight condition. In the flight test, the experimental flight vehicle was carried to an altitude of 39 km by a large scientific balloon and was then dropped. During the subsequent free flight, the vehicle passed through the transonic and subsonic flow regimes and the aeroelasticity parameter C_{AE} for the aeroshell, which represents the ratio of the elastic force to aerodynamic force and is one of the nondimensional parameters of aerodynamic force to define the deformation of an aeroshell [6], was comparable with an actual low-ballistic-coefficient reentry from low Earth orbit (LEO), as described in the following section. Flight data and images of the membrane aeroshell during the free flight were obtained by onboard sensors and transmitted to the ground station by telemetry systems. The flight test had three main objectives, summarized as follows:

1) Develop a flight-test method for an experimental flight vehicle with an actual-size flexible membrane aeroshell, including fabrication of the experimental flight vehicle and development of measurement techniques for flight data.

2) Demonstrate structural durability, aerodynamic stability, and deceleration capability of an actual-size flare-type flexible aeroshell during free flight in which C_{AE} corresponds to that for an actual reentry mission from LEO.

3) Obtain the structural and aerodynamic characteristics of the flare-type membrane aeroshell in free flight and compare these test flight results with results from previous wind-tunnel tests.

II. Overview of Study

A. Feasibility Study Based on Trajectory Simulation

Since 2000, our group has researched and developed a low-ballistic-coefficient reentry system using a flexible aeroshell, focusing on the flare-type membrane aeroshell shown in Fig. 1. The most appealing advantage of a low-ballistic-coefficient reentry system is reduction in the aerodynamic heating during reentry. To emphasize this advantage and to clarify the technical problems in the development, we outline here an example of a mission using the trajectory simulation of a low-ballistic-coefficient reentry vehicle, in which a 100 kg vehicle is recovered from the LEO at an altitude of 400 km. A schematic of the vehicle configuration is shown in the inset of Fig. 2, and the specifications of the vehicle and the initial flight conditions of the trajectory simulation are listed in Table. 1.

Figure 2 shows the relation between the ballistic coefficient and the maximum equilibrium temperature at the stagnation point and on the flare-type aeroshell estimated using the trajectory simulation. The heat flux at the stagnation point and on the flare-type aeroshell was calculated using Tauber's equation [7] and Lees's equation [8], respectively. The emissivity of the vehicle surface was set to 0.8, and the radiation on the aeroshell was assumed to be emitted from both front side and back side.

Results of this trajectory simulation show that aerodynamic heating decreases with decreasing ballistic coefficient, i.e., with increasing diameter of the aeroshell. If the ballistic coefficient is less than 2 kg/m^2, which corresponds to an aeroshell larger than 6 m in diameter, the maximum temperature on the aeroshell is less than 650°C. These results indicate that a vehicle with a flexible aeroshell made of an existing material, such as ZYLON® fiber,[††] can safely reenter and return to Earth from LEO if the aeroshell attached to the reentry vehicle is large enough to counteract the aerodynamic heating. Note that a local peak of the aerodynamic heating due to deformation of the aeroshell was not considered in this estimation. Although further study on the local heating is needed, increasing the diameter of the aeroshell can solve this issue.

Figure 3 shows a reentry trajectory for a ballistic coefficient of 1.0 kg/m^2, which corresponds to a 10-m-diam aeroshell. Time 0 was set as the time of deorbit. The vehicle starts decelerating at an altitude of 100 km and the heat flux is less than 80 kW/m^2, even at the stagnation point. This result confirms that this reentry vehicle with a flare-type membrane aeroshell experiences moderate aerodynamic heating compared with conventional ballistic reentry. The time history of the dynamic pressure is also shown in Fig. 3. Dynamic

[††]Data available online at http://www.toyobo.co.jp/e/seihin/kc/pbo/Technical_Information_2005.pdf [retrieved February 2009].

Table 1 Initial flight conditions and specifications of a vehicle for trajectory simulation

Vehicle mass	100 kg
Capsule diameter	1 m
Curvature radius at stagnation	0.71 m
Flare angle of the aeroshell	45 deg
Aeroshell diameter	Varied (1 to 30 m)
Drag coefficient of the vehicle	1.3
Lift coefficient of the vehicle	0.0
Initial velocity	7668 m/s
Initial altitude	400 km
Initial flight pass angle	3.0 deg

pressure is important in estimating the deformation of the aeroshell, because C_{AE} [represented as follows in Eq. (1)] is one of the nondimensional parameters used to define deformation of a flexible aeroshell:

$$C_{AE} = \frac{L_{ref}\rho_\infty V_\infty^2}{Eh} \tag{1}$$

The trajectory simulation shows that the maximum dynamic pressure is about 0.1 kPa in a low-ballistic-coefficient reentry from LEO.

B. Aim of Our Study

The results of the trajectory simulation indicate that the reentry system using the flare-type membrane aeroshell made of existing flexible material is feasible. The next important technical problem in the development of this reentry system is stability and durability of a flare-type membrane aeroshell in flight conditions based on structural dynamics and aerodynamics. As a first step in our study, a wind-tunnel test using scale models that have a flexible aerodynamic surface [6,9] and Navier–Stokes flow analysis coupled with particle-based membrane structural analysis [9,10] were conducted to investigate the potential of the flare-type membrane aeroshell as a decelerator for a high-speed vehicle such as spacecraft. However, our

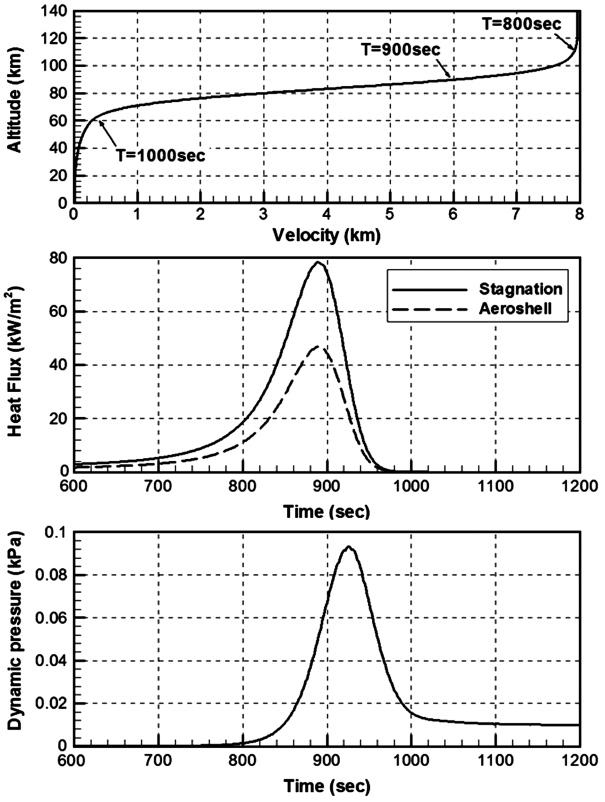

Fig. 3 Aerodynamic environment in the reentry trajectory of the low-ballistic-coefficient vehicle for a ballistic coefficient of 1.0 kg/m².

wind-tunnel tests and numerical simulations did not sufficiently clarify the characteristics of the flexible aeroshell in the transonic and supersonic flow regimes. For example, the thickness and flexural rigidity of the membrane of the flexible aeroshell is expected to affect the deformed shape and aerodynamic characteristics of the aeroshell during flight. Simulating such conditions in wind-tunnel tests using a scale model is impossible, because in an actual space vehicle, the membrane is very thin (on the order of 10^{-3} m) and the ratio of the membrane thickness to the radius of the aeroshell is small (on the order of 10^{-4}).

Based on the scaling law, making a membrane sufficiently thin for a scale model used in a wind tunnel is not realistic. Another difficulty that cannot be resolved in wind-tunnel tests is confirmation of the dynamic stability of vehicle with a flexible aerodynamic surface under complete free-flight conditions. The dynamic stability during free flight must be thoroughly evaluated, because this vehicle has many degrees of freedom, due to the flexibility of the aeroshell itself and resulting deformation. Furthermore, current numerical simulation methods cannot precisely analyze flexible structures consisting of a thin membrane. Even if such numerical simulation were possible, the analysis of the unsteady phenomena, including coupled oscillation with the membrane and flow, would be extremely difficult and would require prohibitive computational cost.

In conclusion, free-flight tests must be conducted to clarify in detail the aerodynamic characteristics of the flexible aeroshell and to demonstrate the stable flight of a capsule-type vehicle with a flexible membrane aeroshell. In particular, the stability of the flare-type membrane aeroshell based on structural dynamics and aerodynamics in the complete free-flight condition can be demonstrated only by flight tests.

III. Experimental Flight Vehicle and Measurement System

A. Experimental Flight Vehicle Configuration

Figure 4 shows a drawing of the experimental flight vehicle used in the flight test. The vehicle consisted of a blunt capsule, a frustum-shaped membrane, and a deployable outer frame. The spherically blunted capsule was made of iron, had a maximum diameter of 600 mm, and had a nose radius of 422 mm. All the sensors, telemetry system, and batteries were installed in the capsule. The membrane aeroshell was made of ZYLON textile, which was chosen for its high heat resistance and strength, although the aerodynamic heating was negligible in this flight test. ZYLON textile is a candidate material for the flexible aeroshell in a future actual reentry mission. A grid pattern was printed on the backside of the membrane aeroshell to enhance the visibility of the deformation of the aeroshell. The outer frame was installed at the outer end of the membrane aeroshell to maintain the configuration of the aeroshell, withstanding the compression force caused by aerodynamic forces during the flight. The configuration of the outer frame was dodecagonal and composed of 12 hollow aluminum pipes. A hinge assembly with a pair of carpenter tapes made of spring steel [11] was installed at the middle of each aluminum pipe. An automatic latching mechanism was added on the carpenter-tape hinge to increase the strength of the outer frame after deployment. The pair of carpenter tapes generated the deployment force when they were folded and increased the rigidity when fully deployed and latched. A preflight ground test confirmed that the fully deployed outer frame could withstand a compression force of up to 1200 N. The configuration of the membrane aeroshell was frustum-shaped with a 45 deg half-angle and 1480 mm in maximum diameter.

In this flight test, the diameter of the aeroshell was set at about 1.5 m, due to constraints in launching of the balloon, although a flexible aeroshell about 10 m in diameter might be required to recover a 100 kg payload from LEO. However, this experimental flight vehicle has an aeroshell that is 15 times larger than that in the scale model used in the preflight wind-tunnel test. The scale effects of the vehicle can be predicated by comparison between the results of the wind-tunnel tests and the flight test. The mass of the capsule, including all equipment, was 102.3 kg; the membrane aeroshell was 0.6 kg; and the outer frame was 2.6 kg. Therefore, the total mass of

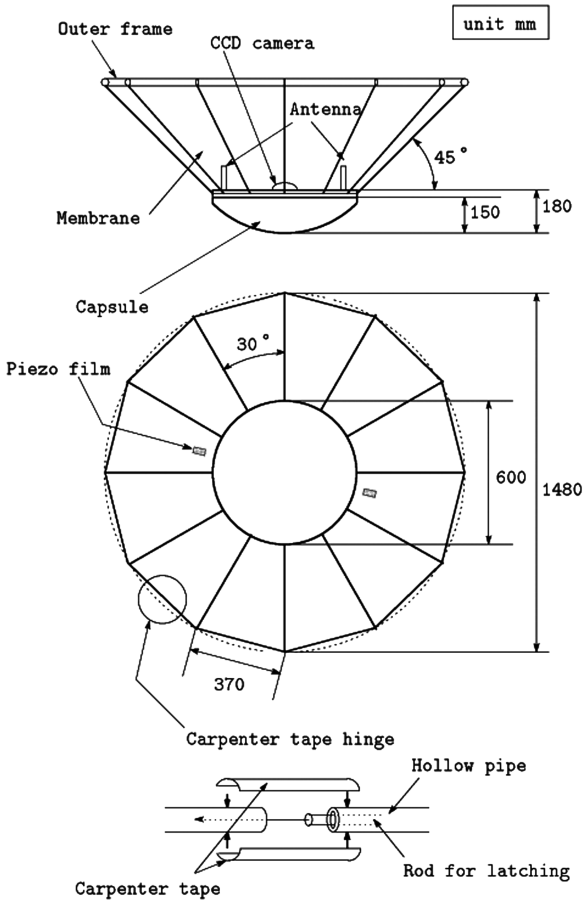

Fig. 4 Drawing of the experimental flight vehicle used in the flight test.

the vehicle was 105.5 kg. The ballistic coefficient of the entire experimental vehicle was approximately 64 kg/m^2, assuming a drag coefficient of 1.0. In this flight test, C_{AE} was set to a range comparable with an actual reentry mission. The membrane aeroshell of the experimental vehicle was made of material that can be used for an actual reentry mission, although the size of the aeroshell was about one-tenth of that for an actual reentry mission. The dynamic pressure required in this flight experiment was 1.0 kPa, because the dynamic pressure is 0.1 kPa in an actual reentry mission, as described in Sec. II.A. The mass of the experimental vehicle was set to achieve 1.0 kPa in dynamic pressure in this flight test.

Table 2 summarizes the specifications of the experimental flight vehicle.

B. Measurement Method

In this flight test, the deformation, oscillation, and drag coefficients of the membrane aeroshell were measured using onboard sensors. The shape of the membrane aeroshell during the free flight was measured based on images obtained using a charge-coupled-device (CCD) camera mounted on the backside of the capsule, thus allowing a 360 deg view of the aeroshell using a fish-eye lens. Figure 5 shows a schematic of the distortion of the fish-eye lens. The relation between the elevation angle from the horizontal plane and the distance of the center of the lens to the projection plane was defined by the following mapping equation:

$$d = 2L_f \tan\frac{\theta}{2} \tag{2}$$

The shape of the membrane aeroshell cannot be determined only from the image through the fish-eye lens, because this image provides only the elevation angle from the horizontal plane of the grid points on the membrane aeroshell. To uniquely determine the shape of the membrane aeroshell from this image, the elongation of the membrane aeroshell was assumed to be negligible, and thus the distances between any two grid points on the membrane aeroshell were assumed to be constant. This assumption is valid because ZYLON has a significantly large Young's modulus (180 GPa), and the tensile stress acting on the ZYLON was expected to be less than 10 MPa in this flight test.

The locations of the grid points were calculated in sequence from the inner edge to the outer frame because the distance between the grid points and the elevation angle were obtained based on the preceding assumption and on the images obtained through the fish-eye lens. The location of the outer grid point is an intersection of the circle that represents a certain distance from the inner grid point and the line that represents a certain elevation angle from the CCD camera. Figure 6 shows a schematic of the method to reproduce the aeroshell shape from images obtained through the fish-eye lens.

The motion of the membrane aeroshell was observed by the CCD camera. Piezo films for which the signal output depends on the extent of its deformation were attached on the backside of the membrane aeroshell near the capsule to measure the frequency of the oscillation of the membrane. The drag coefficient during the free flight was estimated from the aerodynamic forces, the attitude of the vehicle,

Table 2 Experimental flight vehicle specifications

Capsule diameter	600 mm
Capsule mass	102.3 kg
Material	Iron
Aeroshell diameter	1430 mm
Aeroshell mass	0.6 kg
Material	ZYLON
Outer frame mass	2.6 kg
Material	Aluminum
Diameter of pipe	25 mm
Length of panel	370 mm
Maximum vehicle diameter	1480 mm
Total mass	105.5 kg
Ballistic coefficient	64 kg/m^2

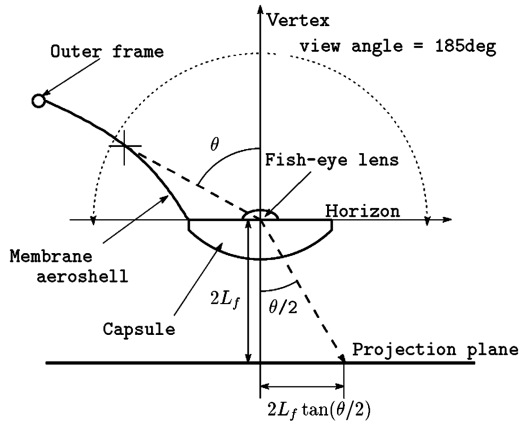

Fig. 5 Distortion of image by fish-eye lens used in the flight test.

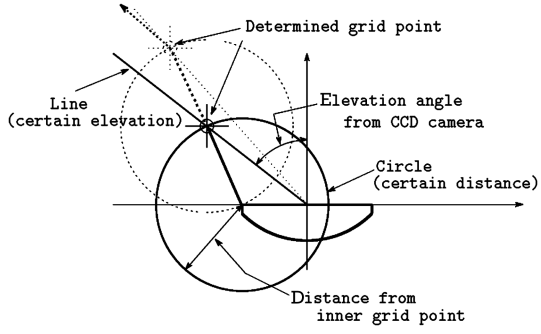

Fig. 6 Method to reproduce the aeroshell shape from images obtained through the fish-eye lens.

Table 3 Onboard sensors used in the flight test

Sensor	Maker	Model number	Comments
CCD camera	SENTECH	STC-630CSII	Pixels: 768 × 494
Fish-eye lens	FIT	FI-085	View angle:185 deg
Acceleration sensor	Xbow	CXL04LP3	Accuracy: ±0.2% full scale
GPS	Furuno	GN-7906A	Accuracy: <0.5 m/s (in velocity)
Pressure sensor	Honeywell	PPT001AWN5VA	Accuracy: ±0.12% full scale
Piezo film	Tokyo Sensor	DT1-052K	——

and the uniform flow condition. The aerodynamic forces were measured by an acceleration sensor. The attitude of the vehicle was determined from the sun elevation obtained from the images of the sun through the fish-eye lens. The uniform flow condition was determined from the vertical velocity, which was calculated from the integration of the vertical acceleration corrected using Global Positioning System (GPS) data and the database containing conditions of the atmosphere at the test site at the Sanriku Balloon Center (SBC).

Table 3 lists the onboard sensors used in this flight test.

IV. Outline of Flight Test

The flight test was carried out using a B100-10 balloon at SBC on 28 August 2004 [12]. The fully expanded volume of a B100 balloon is 100,000 m^3, and this balloon can carry the experimental vehicle tested in this study up to a 39 km altitude. The experimental vehicle was mounted under the gondola, as shown in Fig. 7. All the sensors were turned on and checked before launch. The B100-10 balloon with the vehicle was launched at 0630 hrs. The balloon ascended smoothly and was put into level flight at an altitude of 15 km by opening the exhaust valve and exhausting buoyant gas. When the balloon arrived at a point 200 km eastward offshore, it ascended again by executing a ballast drop, and at 1030 hrs, it reached an altitude of 39 km. Soon after the balloon reached an altitude of 39 km, the vehicle was separated from the gondola and the flight test started at 1040 hrs. The vehicle made an almost vertical downward flight and splashed down 100 km eastward offshore 470 s after this separation. Figure 8 shows a downward-view image of the vehicle captured by a CCD camera equipped on the gondola just after the separation. After the separation, the balloon and gondola continued flight to the east. When the balloon and gondola approached land, the gondola was separated from the balloon and the balloon was broken up. Finally, both the balloon and the gondola were recovered at sea by a ship. Figure 9 shows the trajectories of the B100-10 balloon and the experimental flight vehicle.

V. Results of Flight Test

A. Flight Trajectory

1. Attitude of the Vehicle

First, the attitude of the vehicle was determined. Figure 10 shows an upward-view image taken by the CCD camera with the fish-eye lens mounted on the backside of the capsule. In this view, the balloon and the sun are at the center, and the entire membrane aeroshell is visible. Such images were transmitted at a constant rate of 30 Hz by the telemetry system during the free flight. During the free flight, the sun was always in the images obtained through the fish-eye lens, and thus the attitude of the capsule could be estimated by tracking the position of the sun in the image. Figure 11 shows the track of the sun in the images. The circle with a 1.0 radius represents the boundary of the view through the fish-eye lens. The location of the sun in the image moved on the circular locus with a radius of about 0.3. Based on the distortion of the fish-eye lens, the sun elevation angle estimated from these images ranged from 55 to 65 deg. Based on the location and time of the test flight, the actual sun elevation angle during the flight was about 60 deg. This difference indicates that the inclination of the capsule was less than 5 deg and that the capsule flew at almost vertical attitude during the flight.

Fig. 7 Experimental flight vehicle with the gondola on the launch pad before launch.

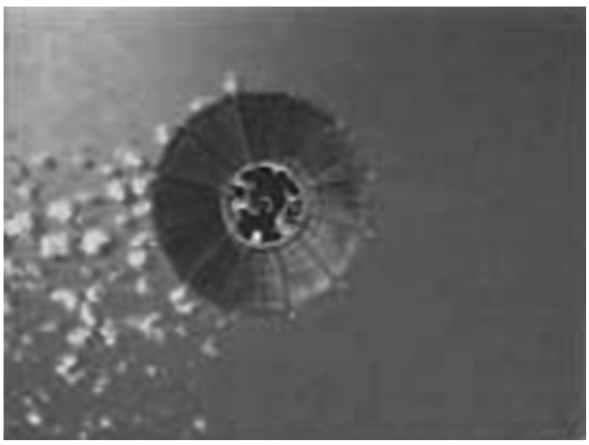

Fig. 8 Downward-view image of the vehicle observed from the gondola just after separation.

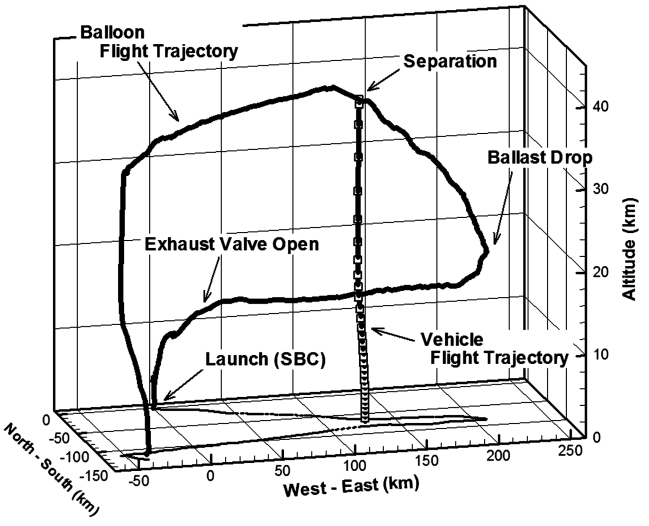

Fig. 9 Flight trajectories of the B100-10 balloon and experimental flight vehicle.

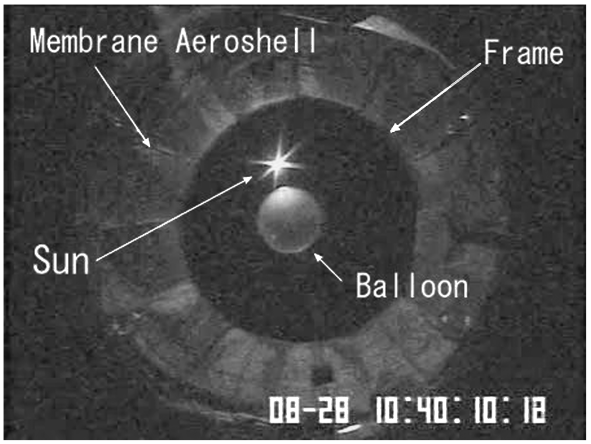

Fig. 10 Upward-view image of the membrane aeroshell through the fish-eye lens just after separation.

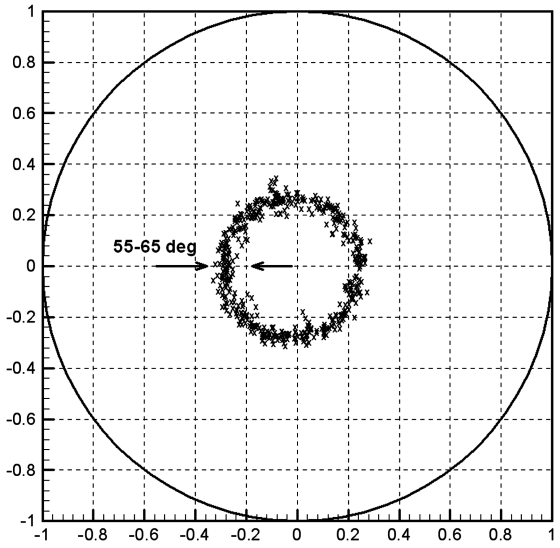

Fig. 11 Position of the sun in the view of the onboard camera with the fish-eye lens.

2. Horizontal Trajectory of the Vehicle

The horizontal trajectory of the vehicle determined based on the GPS data revealed that the vehicle slowly drifted west after the separation and then turned southeast. The horizontal velocity of the vehicle reached 40 m/s, due to the jet stream at an altitude of about 14 km. Finally, the vehicle turned west again just before splashdown. The maximum flight-path angle, which was defined as the angle of the velocity vector of the vehicle from the vertical axis, was 25 deg at an altitude of about 14 km, the horizontal velocity was 40 m/s, and vertical velocity was 70 m/s. Figure 12 shows the horizontal motion of the vehicle, wind direction, and wind velocity during free flight. The wind velocity and direction were determined from the horizontal motion of the B100-10 balloon during the ascent, because the horizontal motion of the balloon corresponds to the wind velocity. The x axis in Fig. 12 is the altitude and the y axes are the horizontal velocity (lower figure) and direction (upper figure) of the wind and the vehicle. Based on these figures, at all altitudes, the horizontal velocity vector coincided with the wind velocity and direction. This means that the vehicle dropped with a vertical attitude at almost a zero angle of attack, although the flight-path angle reached 25 deg.

3. Vertical Trajectory of the Vehicle

Figure 13 shows the time histories of the vertical velocity and the altitude of the vehicle. The vertical velocity was obtained by integration of the vertical acceleration compensated by the GPS data, and the altitude was obtained by integration of the vertical velocity

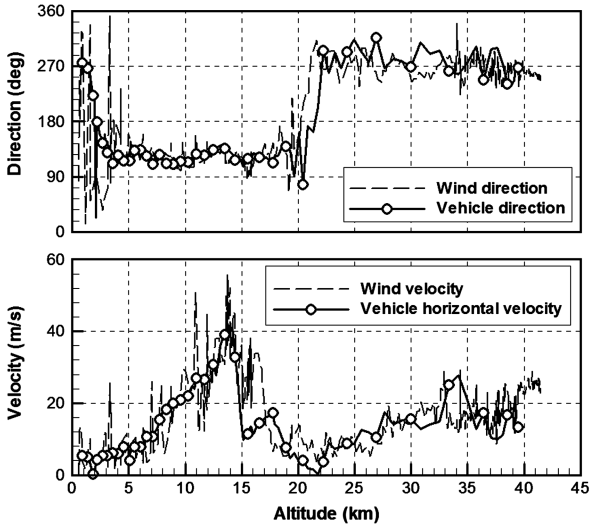

Fig. 12 Comparison of the wind velocity and direction with the flight trajectory.

compensated by the pressure altimeter. To accurately determine the velocity and altitude, the zero point of the acceleration sensor at separation had to be determined, because the simple integration of the output of the acceleration sensor generated a large error, due to the zero drift of the acceleration sensor. In this analysis, the value of the zero drift of the acceleration sensor at the separation was determined based on the comparison between the integration of the vertical acceleration and the time history of the pressure altimeter and velocity of the vehicle obtained from GPS. Figure 13 also shows the time histories of the dynamic pressure and the Mach number. Flight conditions were estimated based on a database containing average atmospheric conditions observed using sounding sondes and sounding rockets at the Sanriku region for several years.

The velocity of the vehicle reached a maximum speed of 280 m/s (Mach number 0.94) at 40 s after separation. The vehicle splashed down 470 s after separation with a terminal velocity of 31 m/s. The vehicle experienced a maximum dynamic pressure of 0.84 kPa about 60 s after separation. Figure 13 also shows the predicted trajectory computed based on a one-dimensional point-mass system. In this computation, the relation between the drag coefficient and the Mach number of the vehicle was defined according to the results of

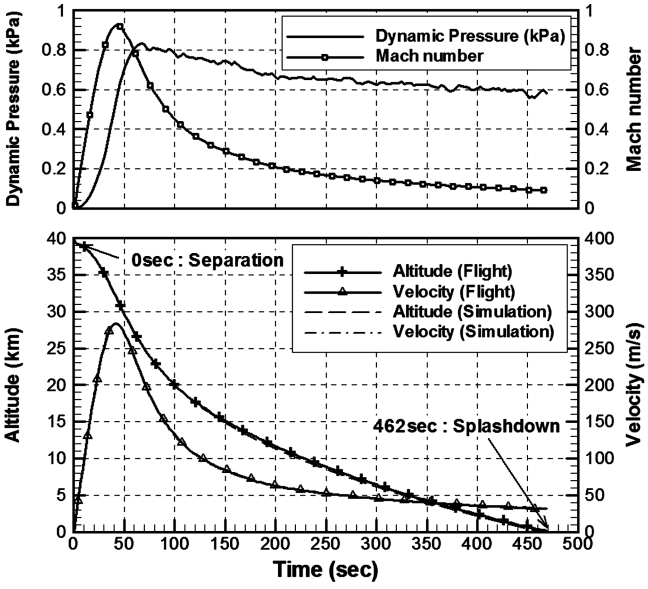

Fig. 13 Time histories of altitude, velocity, Mach number and dynamic pressure during free flight based on flight data measurements and on simulation of trajectory analysis.

transonic wind-tunnel tests [13]. The flight path was almost identical to the predicted trajectory, indicating that the actual drag force during the free flight can be predicted well by using data of the drag coefficient obtained by wind-tunnel tests, as discussed in Sec. V.B.

B. Estimation of Drag Coefficient from Flight Data

From flight data, the drag coefficient of the vehicle was calculated as follows:

$$C_D = \frac{ma_z}{\frac{1}{2}\rho_\infty V_z^2 S_{\text{ref}}} \tag{3}$$

Figure 14 shows the relation between Mach number and drag coefficient C_D obtained from flight data averaged at Mach number intervals of 0.1. The estimated error in the drag coefficient determined from this flight data was 10%, in which the dominant contributor was the error in the atmospheric density (about 5%), due to temporal fluctuation and spatial variation of the atmosphere. Error in the measured vertical velocity depended on the accuracy of the GPS and was estimated at 1–2%. Errors in the measured mass of the vehicle, reference area, and acceleration sensors were all less than 1% each. Figure 14 also shows the results from the subsonic and transonic wind-tunnel tests [13]. The angle of attack was 0 deg from the wind-tunnel data, and almost 0 deg from the free-flight-test data (see Sec. V.A.1).

Both the flight-test data and the wind-tunnel data show that the drag coefficient was 0.9–1.0 in the subsonic flow regime, increased with increasing Mach number, and reached 1.15 at Mach number 0.9. The results in the flight test are in good agreement with the results of the wind-tunnel tests, despite differences in aerodynamic conditions: for example, dynamic pressure and Reynolds number. The dynamic pressure is an important parameter because it is proportional to C_{AE}, which is one of the nondimensional parameters used to define the deformation of the flexible aeroshell. However, the effect of the dynamic pressure was not significant for our experimental vehicle, because ZYLON textile is sufficiently strong and the elastic force is significantly larger than the aerodynamic force, and so elongation of the membrane can be ignored. The Reynolds number in this flight test ranged from $0.5–3.0 \times 10^6$, whereas in the wind-tunnel test, it ranged from $1.0–2.0 \times 10^6$. The variation in Reynolds number did not significantly affect the capability of deceleration by this aeroshell. Therefore, as expected from the wind-tunnel tests, the flare-type membrane aeroshell has a reasonable capability as a decelerator in free flight. Furthermore, the drag coefficient of the flare-type membrane aeroshell in free flight can be predicted by wind-tunnel tests.

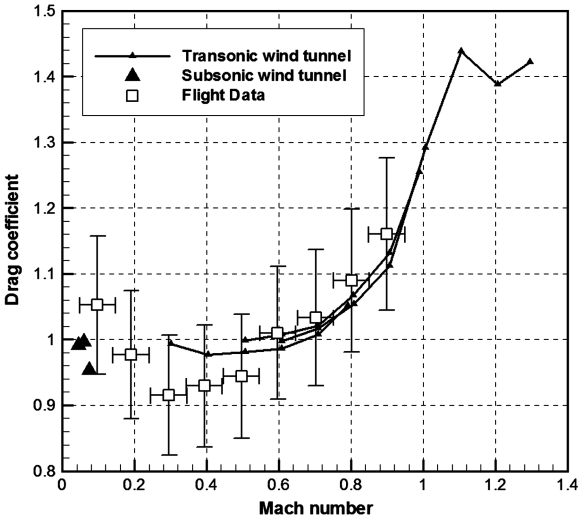

Fig. 14 Drag coefficient as a function of Mach number based on measured flight data and on subsonic and transonic wind-tunnel tests.

C. Deformation of the Aeroshell During Free Flight

Images obtained by the CCD camera installed on the backside of the capsule confirmed that, except for a small oscillation, the membrane aeroshell maintained its shape during the free flight. Figures 15a and 15b show two representative images used to estimate the deformation of the membrane aeroshell based on the method described in Sec. III.B and shown in Fig. 6. Figure 15a was captured 60 s after separation, when the dynamic pressure reached a maximum, and Fig. 15b was captured before the flight test under no-wind conditions (i.e., unloaded condition), in which the outer frame attached to the outer edge of the aeroshell simply hung and the membrane was conical-shaped, due only to the mass of the capsule.

Figure 15c shows the reproduced shape of the membrane aeroshell under both conditions. The reproduced shape of the membrane aeroshell under unloaded conditions was slightly curved, although the shape of the membrane aeroshell was designed to be conical, as indicated by the gray straight line in Fig. 15c. The discrepancy between the design shape and reproduced shape is less than 3 cm, indicating that this reproduction method is sufficiently accurate for qualitative discussion about the deformation of the membrane aeroshell.

The reproduced shape during the free flight (Fig. 15c) shows that the membrane near the capsule was deformed along the freestream and that the outer part was deformed vertically against the freestream. Thus, the membrane aeroshell was deformed into a concave shape due to aerodynamic forces. Wrinkles were observed in the radial direction on the membrane aeroshell, and the outer frame was hidden by the membrane in the image during the flight (Fig. 15a), because the membrane aeroshell became concave and the middle part of the aeroshell was compressed in the circumferential direction. Such qualitative characteristics of the deformed shape were as expected, based on the wind-tunnel tests [13] and numerical simulations [10], as shown in Fig. 16.

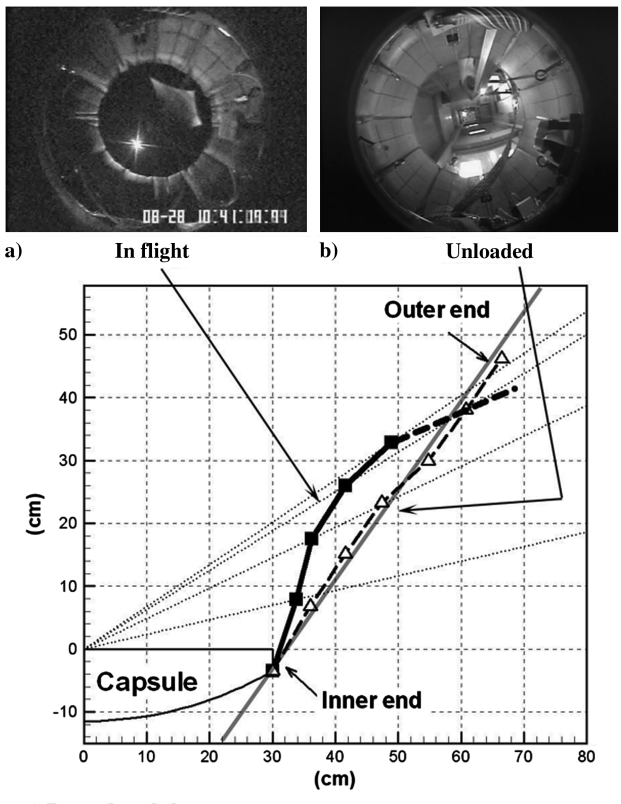

c) Reproduced shapes

Fig. 15 Deformed shape of the membrane aeroshell estimated from images obtained through the fish-eye lens: a) Image during the free flight, b) image under unloaded condition, and c) reproduced shapes.

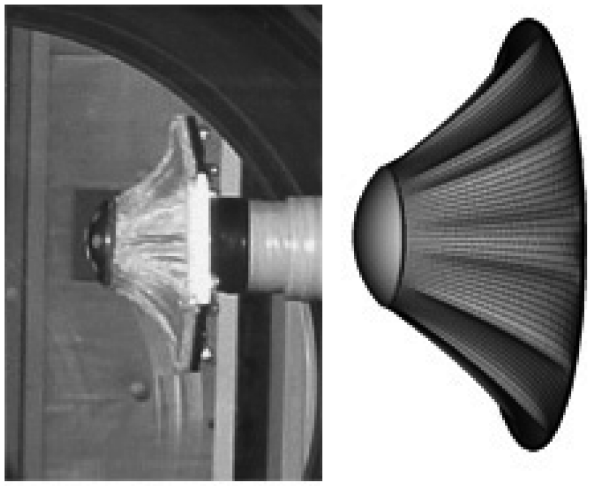

a) b)

Fig. 16 Deformed shape of the flare-type membrane aeroshell obtained by the wind-tunnel test and the numerical simulation: a) scale model of the flare-type membrane aeroshell used in transonic wind-tunnel tests at Mach number 0.9 and b) resultant shape of the conical flexible aeroshell based on numerical simulation using the particle-based membrane model and Newtonian flow approximation.

D. Oscillation of the Membrane During Free Flight

A slight oscillation of the membrane aeroshell was observed in the images obtained using the CCD camera. For 150 s after separation, the entire aeroshell oscillated around the center axis of the capsule randomly, as shown in the drawing in the upper right in Fig. 17. The frequency of this aeroshell oscillation was approximately 4 Hz. About 250 s after separation and continuing until splashdown, the membrane fluttered, as shown in the upper left in Fig. 17. The frequency of this membrane fluttering was approximately 10 Hz.

The aeroshell oscillation and membrane fluttering were also detected by the piezo films attached on the membrane aeroshell. To investigate the temporal variation in frequency intensity, we divided the total flight period into 35 sectors for convenience of analysis, and then the output of the piezo film at each sector was analyzed using fast Fourier transform (FFT). The sampling rate of the output of each piezo film was 85 Hz, which was fast enough for analysis of the aeroshell oscillation and membrane fluttering. Figure 17 shows the contours of the intensity on the plane of the Mach number (x axis) and the frequency of the oscillation (y axis), indicating that the piezo film detected both the aeroshell oscillation and membrane fluttering.

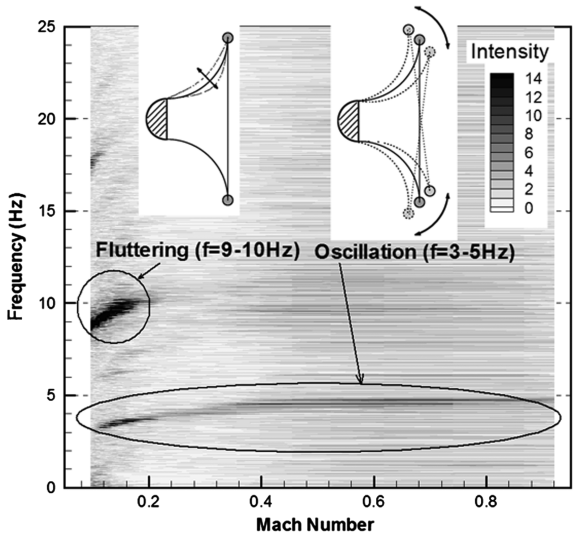

Fig. 17 Aeroshell oscillation and membrane fluttering based on FFT analysis of the output of piezo films on the membrane aeroshell.

The intensity of the aeroshell oscillation was dominant at the frequency of 4 Hz when the Mach number was more than 0.2, whereas when the Mach number was less than 0.2, the intensity of the membrane fluttering at the frequency of 10 Hz became dominant. This result indicates that the change in oscillation mode observed 250 s after separation was caused by the onset of the membrane fluttering, which was more significant than the aeroshell oscillation when the Mach number was less than 0.2.

The Strouhal numbers of the oscillation and fluttering in the subsonic regime were calculated using the terminal velocity as follows:

$$St = \frac{fL_{\text{ref}}}{V_{\text{ter}}} \tag{4}$$

The Strouhal numbers of the aeroshell oscillation and membrane fluttering were 0.14 and 0.43, respectively, which are similar to Strouhal numbers on the frequency of the Kármán vortex generated in the wake of a cylinder (0.2). Hence, these two motions of the membrane aeroshell might be coupled with the unsteady flow in the wake of the vehicle. Further study is needed to quantify the relation between the flow around the vehicle and the motion of the flexible membrane aeroshell by comparing wind-tunnel tests and numerical simulations.

VI. Conclusions

The flight test of a capsule with a flare-type flexible membrane aeroshell was carried out successfully using a large scientific balloon. This flight test was the first step in the development of a flexible membrane aeroshell for a reentry system.

For this flight test, an actual-scale model was fabricated, including various sensors, telemetry system, and batteries. During the flight test, flight data for the trajectory and attitude of the vehicle and images of the flexible aeroshell during the free flight were obtained. The flight data confirmed that, except for the oscillation and fluttering of the aeroshell, the vehicle held a stable vertical attitude and attained a descent with almost zero angle of attack. These results demonstrated the decelerating capability of the flare-type membrane aeroshell during free flight. The relation between the Mach number and the drag coefficient obtained from the flight data agreed well with previous results from wind-tunnel tests, and the concavely deformed shape of the aeroshell during the flight was also observed in both the wind-tunnel tests and the numerical simulation. This flight test clearly demonstrated the aerodynamic capability of the flare-type thin-membrane aeroshell for an atmospheric-entry vehicle. However, before this flexible aeroshell can be applied to an actual atmospheric-entry mission, several issues need to be resolved: for example, the durability of the flexible material against aerodynamic heating during atmospheric-entry, the development of a larger but lighter flexible aeroshell, and clarification of the aerodynamic characteristics in the hypersonic flow regime. To resolve these issues, future wind-tunnel test methods and numerical simulations for this vehicle with membrane aeroshell will be improved based on the results of this flight test. The experimental vehicle will be designed using the results of wind-tunnel test, and the numerical simulation and flight demonstrations will be conducted under more realistic reentry conditions using a balloon, a sounding rocket, or a satellite.

Acknowledgments

The authors would like to acknowledge the following individuals, agency, and company for their contributions during the development of this experimental flight vehicle and the operation of this flight test: Yuuki Tsutsumi, Kazuhiko Wakatsuki (Tokai University), Keisuke Kinumoto, Daiki Sadamitsu, Kunihiko Sugamuma, Yoshiki Takama, Kumiko Nakamura, Kohmei Hanada, Yuugo Hiura, (University of Tokyo), Akira Sakurai (Kyushu University), Scientific Balloon Center, Institute of Space and Astronautical Science, Japan Aerospace Exploration Agency, and Toyobo Co., Ltd.

References

[1] Iannotta, B., "Down-to-Earth: Transport for Space Cargo," *Aerospace America*, July 2000, pp. 39–42.

[2] Rohrschneider, R., R., and Braun, R., D., "Survey of Ballute Technology for Aerocapture," *Journal of Spacecraft and Rockets*, Vol. 44, No. 1, Jan.–Feb. 2007, pp. 10–23. doi:10.2514/1.19288

[3] Gräßilin, M., and Schöttle, U., "Flight Performance Evaluation of the Reentry Mission IRDT-1," International Aeronautical Federation Paper IAF-01-v.3.05, Oct. 2001.

[4] Hughes, S. J., Dillman, R. A., Starr, B. R., Stephan, R. A., Lindell, M. C., Player, C. J., and Cheatwood, F. M., "Inflatable Reentry Vehicle Experiment (IRVE) Design Overview," AIAA Paper 2005-1636, 2005.

[5] Anderson, M. S., Robinsion, J. C., Bush, H. G., and Fralich, R. W., "A Tension Shell Structure for Application to Entry Vehicles," NASA, TN D-2675, Mar. 1965.

[6] Yamada, K., Suzuki, K., and Hongo, M., "Aerodynamic Characteristics of Frustum-Shaped Elastic Membrane Aeroshells in Supersonic Flow," *Journal of Spacecraft and Rockets*, Vol. 43, No. 3, 2006, pp. 690–693. doi:10.2514/1.15901

[7] Tauber, M. E., Bowles, J. V., and Lily, Yang, "Use of Atmospheric Braking During Mars Missions," *Journal of Spacecraft and Rockets*, Vol. 27, No. 5, Sept.–Oct. 1990, pp. 514–521. doi:10.2514/3.26174

[8] Lester, L., "Laminar Heat Transfer over Blunt-Nosed Bodies at Hypersonic Flight Speeds," *Jet Propulsion*, Vol. 26, No. 4, Apr. 1956, pp. 259–269.

[9] Yamada, K., "Study on the Aerodynamic Characteristic of the membrane Aeroshell in Supersonic Flow and Its Application to Low-Ballistic-Coefficient Reentry Vehicle," Ph.D. Thesis, Univ. of Tokyo, Tokyo, 2004 (in Japanese).

[10] Yamada, K., and Suzuki, K., "A Particle-based Model and Its Validation for Deformation Analysis of the Membrane Aeroshell," *Journal of the Japan Society for Aeronautical and Space Sciences*, Vol. 53, No. 613, 2005, pp. 51–60. doi:10.2322/jjsass.53.51 (in Japanese).

[11] Feria, V. A., Lou, M. C., Huang, J., and Speer, S. E., "Lightweight Deployable Space Radar Array," AIAA Paper 98-1933, 1998, pp. 1871–1875.

[12] Yamada, K., Akita, D., Sato, E., Suzuki, K., Tsutsumi, Y., Wakatuski, K., Narumi, T., Sakurai, A., Abe, T., and Matsusaka, Y., "Flight Experiment of the Capsule with the Deployable Flexible Aeroshell Using a Large Scientific Balloon," International Astronautical Congress Paper 05-D2.6.05, 2005.

[13] Sato, E., Yamada, K., Suzuki, K., Abe, T., Akita, D., Nakazawa, E., Kiuchi, M., Tsutsumi, Y., Wakatsuki, K., Sakurai, A., Narumi, T., Matsusaka, Y., and Iijima, I., "Flight Experiment of Capsule-Type Vehicle with Membrane Aeroshell by Means of Large Scientific Balloon," International Symposium on Space Technology and Science, Paper 2004-g-10, 2004.

J. Martin
Associate Editor